Demethylation of dextromethorphan/levomethorphan in rat and human liver microsomes

For the *in vitro* experiments with rat and human liver microsomes, the reaction mixture consisted of 0.1 M potassium phosphate buffer (pH 7.4) with an NADPH generating system (1.3 mM NADP, 3.3 mM G-6-P, 0.4 U/mL G-6-PDH, 3.3 mM $MgCl_2$), 50 μM substrate (dextromethorphan or levomethorphan), and 0.5 mg protein/mL microsomes (rat or human liver microsomes) in a final volume of 200 μL. Dextromethorphan and levomethorphan were dissolved in methanol, and the final concentration of the organic solvent was 0.1%. The incubation was started by adding the microsomal fraction and then continued for 0, 5, 10, or 20 min. The reaction was terminated by adding an equal volume of a mixed organic solution of 50% acetonitrile and 50% methanol, including 10 μM levallorphan (IS), and vigorous shaking. At the same time, a reaction mixture without the microsomal fraction was also incubated as an enzyme-free control. The mixture was centrifuged at 3,500×*g* for 3 min at 4 °C, and the supernatant was filtered prior to the injection for the LC-MS/MS analysis. The *in vitro* experiments for kinetic analyses were also performed as described above, except that 2, 5, 10, 50, 100, and 150 μM of substrates were incubated with the rat and human liver microsomes for 10 min. Each experiment was performed in duplicate and kinetic parameters were calculated with Eadie–Hofstee plots.

The results of the *in vitro* experiments were each evaluated by three consecutive analyses. The amounts of dextromethorphan/levomethorphan and their metabolites were calculated on the basis of calibration curves made by spiking known amounts of these compounds into the reaction mixture without the microsomal fraction.

Results

Chiral separation of dextromethorphan/levomethorphan and their metabolites

Complete chiral separation of dextromethorphan, levomethorphan, and their metabolites was achieved in 12 min on a Chiral CD-Ph column in 0.1% formic acid–acetonitrile by a linear gradient program. The retention time of each compound was as follows: the parent compounds (dextro/levo forms, 10.6/11.3 min) and their metabolites of *O*-demethyl (6.1/5.5 min), *N*-demethyl (8.1/9.8 min), and *O*, *N*-didemethyl (3.9/4.5 min) as shown in Table 1. Figure 3 shows LC-MS/MS total ion current chromatograms (MRM mode) of the extract from plasma (30 min after the first administration), urine (0–24 h after the last administration), and hair (collected 4 weeks after the first administration) of rats administered with dextromethorphan or levomethorphan. Under the chromatographic conditions used, there was no interference with any of the compounds or the internal standard by any extractable endogenous materials in the rat samples. The peaks 7 (9.8 min, *m/z* 258→170) and 8 (4.5 min, *m/z* 244→156) on the chromatograms shown in Fig. 3 were identified as those of (−)-3-MEM and (−)-3-HM when the mass fragmentations of these peaks were considered, although the standard compounds of these two metabolites were not available. These peaks were also confirmed by comparison of their retention times and mass fragmentations with those of the standard compounds of the dextro forms ((+)-3-MEM and (+)-3-HM) using an ODS column.

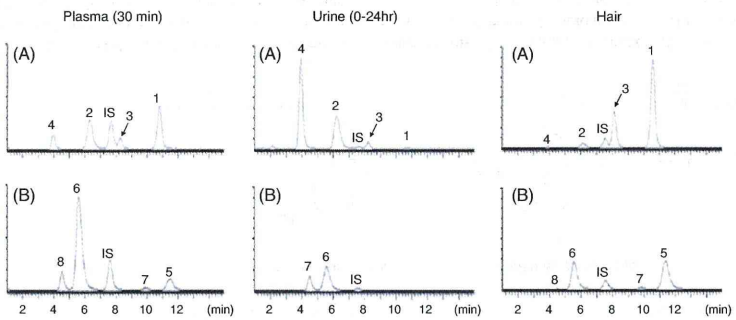

Fig. 3 LC-MS/MS total ion current (TIC) chromatograms (MRM mode) of the extracts from plasma, urine, and hair of rats administered with (**A**) dextromethorphan and (**B**) levomethorphan using a chiral column. *1* Dextromethorphan, *2* Dextrorphan, *3* (+)-3-MEM, *4* (+)-3-HM, *5* Levomethorphan, *6* Levorphanol, *7* (−)-3-MEM, *8* (−)-3-HM

Table 2 Validation of results of the LC-MS/MS analyses of dextromethorphan/levomethorphan and their metabolites in rat plasma, urine and hair samples (n=5)

Samples		Compounds	LOD (S/N>3)	LOQ (S/N>10)	Linear ranges	Recoveries (%)	Precision (%) (n=5)			Accuracy (%) (n=5)		
			(ng/mL)			80 ng/mL	2.0 ng/mL	20 ng/mL	200 ng/mL	2.0 ng/mL	20 ng/mL	200 ng/mL
Plasma (50 μL)		Dextromethorphan	0.8	1.0		106.1	22.1	9.3	1.5	-19.2	5.5	-0.2
	Dextro	Dextrorphan	0.4	0.8	1.0-400	81.7	10.2	3.8	1.5	10.2	2.2	-3.6
		(+)-3-MEM	0.8	1.0		110.5	15.0	3.2	2.5	23.5	2.1	2.6
		(+)-3-HM	0.8	1.0		92.5	15.7	6.1	1.8	13.7	-8.3	2.9
	Levo	Levomethorphan	0.8	1.0	1.0-400	100.8	8.6	4.9	2.5	21.6	-4.4	-5.7
		Levorphanol	0.8	1.0		90.7	15.9	4.1	2.3	-10.6	-5.6	-3.6
			(ng/mL)			500 ng/mL	5.0 ng/mL	500 ng/mL	5000 ng/mL	5.0 ng/mL	500 ng/mL	5000 ng/mL
Urine (100 μL)		Dextromethorphan	1.0	2.5		90.2	9.7	0.8	2.6	-4.8	-5.2	-4.8
	Dextro	Dextrorphan	1.0	2.5	5.0-10000	106.1	23.6	4.6	3.2	-17.9	11.1	-3.3
		(+)-3-MEM	2.5	5.0		102.5	19.7	6.1	4.2	10.4	-5.8	2.7
		(+)-3-HM	2.5	5.0		91.3	24.6	5.1	2.6	1.6	-9.9	1.5
							10 ng/mL			10 ng/mL		
	Levo	Levomethorphan	1.0	5.0	10-10000	94.6	10.9	9.5	2.6	-4.3	-17.0	-2.2
		Levorphanol	1.0	5.0		93.1	4.8	4.5	4.6	18.6	-8.0	6.8
			(ng/mg)			10 ng/mg	0.1 ng/mg	5.0 ng/mg	50 ng/mg	0.1 ng/mg	5.0 ng/mg	50 ng/mg
Hair (10 mg)		Dextromethorphan	0.025	0.05		84.2	11.5	4.5	2.8	4.6	18.8	-6.6
	Dextro	Dextrorphan	0.025	0.05	0.1-50	99.8	6.4	2.6	2.7	3.7	15.4	-3.5
		(+)-3-MEM	0.025	0.05		83.8	18.6	3.9	1.5	4.7	0.6	-2.2
		(+)-3-HM	0.025	0.1		91.4	11.2	6.2	2.8	4.6	18.8	-6.6
	Levo	Levomethorphan	0.025	0.1	0.1-50	98.1	9.9	9.8	5.5	0.1	-2.3	-5.1
		Levorphanol	0.025	0.05		112.2	8.8	2.8	4.2	11.9	1.3	-3.8

Linearity and precision of the analytical method for the rat urine, plasma, and hair samples

The calibration curves were linear over the concentration range 1.0–400 ng/mL for rat plasma, 5.0–10,000 ng/mL (compounds of dextro forms) and 10.0–10,000 ng/mL (compounds of levo forms) for rat urine, and 0.1–50 ng/mg for rat hair, with good correlation coefficients of $r^2 \geq 0.996$, respectively. The LOD of each drug was 0.4 or 0.8 ng/mL for the plasma, 1.0 or 2.5 ng/mL for the urine, and 25 pg/mg for the hair samples. The recoveries and the precision and accuracy data from the analytical procedures for the rat samples (n=5), spiked with a standard solution of the targeted compounds, are shown in Table 2.

Determination of dextromethorphan/levomethorphan and their metabolites in DA rat plasma, urine, and hair samples

It has been reported that a female DA rat lacks the CYP2D1 enzyme, which is known to be related to *O*-demethylation of dextromethorphan in the SD rat; it is therefore used as a model animal for the poor metabolizer phenotype of dextromethorphan [35–37]. As such, the metabolic data from female DA rats may not reflect the "normal" situation. On the other hand, pigmented hairy rats appear to be suitable for the investigation of analytical methods of basic drugs in hair samples, compared with albino rats (SD or Wistar rats) because pigmentation (the melanin contents) is one of the most important factors regarding the incorporation of basic drugs into hair, as described before [38]. Therefore, thus far, we have studied the analytical properties of various drugs in hair samples using the pigmented hairy male DA rats, avoiding female DA rats.

After the i.p. administration of dextromethorphan or levomethorphan to pigmented hairy male DA rats, the parent compounds and their three metabolites in the plasma, urine, and hair were determined using LC-MS/MS. The optical purities of the resulting metabolites were unchanged in any rat biological sample, and no racemation was observed through *O*- and/or *N*-demethylation (Fig. 3). In the rat plasma ($AUCs_{0\text{–}360\ min}$) and urine samples (total excretions for 0–72 h) after the hydrolysis of *O*-glucuronides, most metabolites were detected as being the corresponding *O*-demethyl and *N*, *O*-didemethyl compounds, as shown in Table 3. However, obvious differences in the amounts of these metabolites were found between the dextro and levo forms. After administration of dextromethorphan, dextrorphan and (+)-3-HM were the major metabolites in the plasma (59.4 and 64.3 mg/L·min) and urine (106.1 and 226.9 μg/mL). However, *O*-demethyl metabolites (levorphanol) were mainly detected in the plasma (197.1 mg/L·min) and urine (210.5 μg/mL) after administration of levomethorphan (Table 3).

In the hair samples, the differences in the amounts of the metabolites are more clearly detected. After administration of dextromethorphan, the parent compound and the *N*-demethyl metabolite ((+)-3-MEM) were mainly detected at 63.4 and 25.1 ng/mg, respectively, although the *O*-demethyl metabolite of dextromethorphan (dextrorphan) was detected at only 2.70 ng/mg, which was nearly one tenth of the level

Table 3 Rat plasma $AUCs_{0\text{-}360min}$, total excretion into rat urine, and concentrations in rat hair of dextromethorphan/levomethorphan and their metabolites

Administrations	Targeted compounds	Plasma $AUC_{0\text{-}360min}$ (mg/L·min)	Urine Total excretion 0–72 h (μg)	Hair Concentration (ng/mg)
Dextromethorphan (rat 1–3)	Dextromethorphan	23.8±17.6	2.13±1.05	63.4±4.6
	Dextrorphan	59.4±16.3	106.1±15.3	2.70±0.04
	(+)-3-MEM	3.10±2.15	6.95±0.68	25.1±1.9
	(+)-3-HM	64.3±31.3	226.9±51.3	0.70±0.11
Levomethorphan (rat 4–6)	Levomethorphan	6.90±5.12	0.59±0.61	24.5±5.3
	Levorphanol	197.1±48.2	210.5±36.2	24.6±2.4
	(−)-3-MEM	1.47±0.64	0.13±0.06	2.57±0.71
	(−)-3-HM	51.5±9.6	39.0±5.9	0.49±0.09

of levorphanol. In contrast, after the administration of levomethorphan, the parent compound and the *O*-demethyl metabolite (levorphanol) were mainly detected at 24.5 and 24.6 ng/mg, respectively, with a small amount of the *N*-demethyl metabolite ((−)-3-MEM). The *N*, *O*-didemethyl metabolites (3-HM) were hardly detected in either sample (Table 3). The ratios of the parent compounds, their *O*-demethyl, *N*-demethyl, and *N*, *O*-didemethyl metabolites in the hair samples were 100:4:40:1 for the dextro forms and 100:100:11:2 for the levo forms, respectively.

The rat plasma AUCs, total excretions into rat urine and concentrations in rat hair of dextromethorphan or levomethorphan, and their metabolites are summarized in Fig. 4. The metabolic ratios of dextromethorphan/levomethorphan, *O*-demethyl, *N*-demethyl, and *N*, *O*-didemethyl metabolites in rat plasma ($AUC_{0\text{-}360\ min}$) and hair (collected 4 weeks after the first administration) were 1:3:0.1:3 and 1:0.04:0.4:0.01 for the dextro forms and 1:29:0.2:7 and 1:1:0.1:0.02 for the levo forms, respectively. It is of interest that the concentrations of dextromethorphan and levomethorphan in the rat hair were obviously high compared with those in the plasma, while those of their *O*-demethyl and *N*, *O*-didemethyl metabolites in the hair (which mostly existed as very hydrophilic metabolites, *O*-glucuronides in the plasma) were extremely low considering their high plasma AUCs.

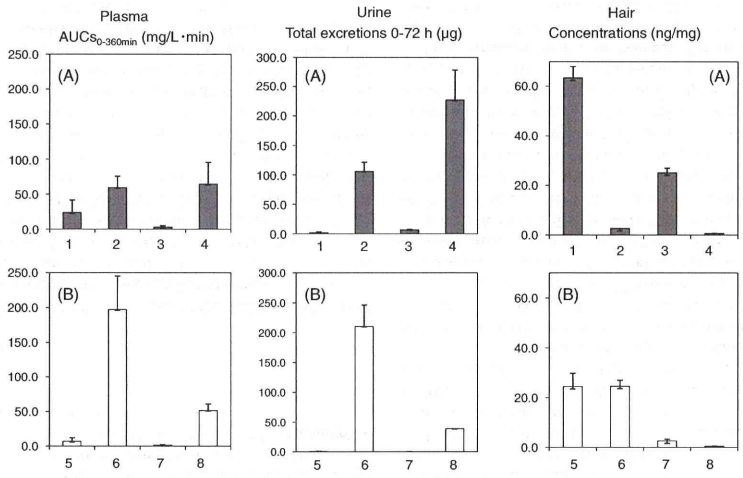

Fig. 4 Rat plasma $AUCs_{0\text{-}360min}$, total excretions into rat urine, and concentrations in rat hair of parent compounds and their metabolites after administration of (**A**) dextromethorphan and (**B**) levomethorphan. *1* Dextromethorphan, *2* Dextrorphan, *3* (+)-3-MEM, *4* (+)-3-HM, *5* Levomethorphan, *6* Levorphanol, *7* (−)-3-MEM, *8* (−)-3-HM

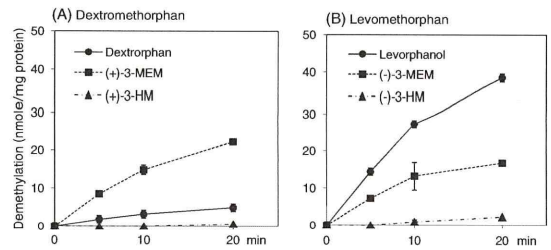

Fig. 5 Demethylation of (**A**) dextromethorphan and (**B**) levomethorphan in DA rat liver microsomes

Demethylation of dextromethorphan/levomethorphan in DA rat liver microsomes

In order to fully investigate the differences of the metabolic properties between dextromethorphan and levomethorphan, DA rat liver microsomes were studied. Figure 5 shows the *O*- and/or *N*-demethylation of dextromethorphan/levomethorphan in the rat liver microsomes.

The optical purities of the resulting metabolites were unchanged in the liver microsomes, and no racemation was observed through *O*- and/or *N*-demethylation. After 20-min incubation, 4.8% of dextromethorphan and 45% of levomethorphan were transformed to each *O*-demethyl metabolite, and 22% and 19% of the parent compounds were transformed to each *N*-demethyl metabolite. The *N*-demethylation was preferred over *O*-demethylation for dextromethorphan. In contrast, *O*-demethylation was preferred over *N*-demethylation for levomethorphan and the *O*-demethylation of levomethorphan was performed at levels 9.4 times that of dextromethorphan after 20-min incubation. The *N*-demethylation of levomethorphan was almost the same as that of dextromethorphan. Table 4 shows kinetic parameters for *O*-demethylation of dextromethorphan and levomethorphan by the DA rat microsomes. The V_{max} value for levomethorphan (3.8±0.3 nmol/min/mg protein) was 5.9 times higher than that of dextromethorphan (0.65±0.03 nmol/min/mg protein). The K_m values for levomethorphan and dextromethorphan were 22.1±5.0 and 44.1±4.0 μM, respectively. These results suggest that there might be an enantioselective *O*-demethylation of levomethorphan in the DA rat liver microsomes. This enantioselective metabolism might be the cause of the different amounts of the metabolites observed in the rat plasma, urine, and hair after administration of dextromethorphan and levomethorphan.

Demethylation of dextromethorphan/levomethorphan in pooled human liver microsomes

In order to investigate whether the enantioselective metabolism could be observed in humans as well as in DA rats, the pooled human liver microsomes were examined. Figure 6 shows the *O*- and/or *N*-demethylation of dextromethorphan/levomethorphan in the human liver microsomes.

The optical purities of the resulting metabolites were unchanged also in the human liver microsomes, and no racemation was observed through *O*- and/or *N*-demethylation. After 20-min incubation, 3.3% of dextromethorphan and 11% of levomethorphan were transformed to each *O*-demethyl metabolite and 2.5% and 7.1% of the parent compounds were transformed to each *N*-demethyl metabolite. The total amounts of the three metabolites from levomethorphan were higher than those from dextromethorphan in human (3.1 times) microsomes. Kinetic parameters for *O*-demethylation of dextromethorphan and

Table 4 Kinetic parameters for *O*-demethylation of dextromethorphan/levomethorphan by DA rat and human liver microsomes

	DA rat liver microsomes		Human liver microsomes	
	Dextromethorphan	Levomethorphan	Dextromethorphan	Levomethorphan
V_{max} (nmol/min/mg protein)	0.65±0.03	3.8±0.3[a]	0.26±0.03	0.58±0.02[a]
K_m (μM)	44.1±4.0	22.1±5.0[a]	4.5±0.9	8.9±1.7[a]

[a] Significantly different from dextromethorphan ($p<0.01$)

levomethorphan in the human liver microsomes are listed in Table 4. The V_{max} value for levomethorphan (0.58±0.02 nmol/min/mg protein) was 2.2 times higher than that of dextromethorphan (0.26±0.03 nmol/min/mg protein). The K_m values for levomethorphan and dextromethorphan were 8.9±1.7 and 4.5±0.8 μM, respectively. There could also be an enantioselective metabolism of levomethorphan in human liver microsomes.

Discussion

In this study, we first investigated the analytical methods of dextromethorphan/levomethorphan and their metabolites in biological samples using DA male rats. As a result, chiral separation of dextromethorphan, levomethorphan, and their metabolites in biological samples was achieved in 12 min on a Chiral CD-Ph column. The optical purities of the resulting metabolites were unchanged in all rat biological samples, and no racemation was observed through *O*- and/or *N*-demethylation. The proposed chiral analyses might be applied to human samples and could provide useful information for discriminating dextromethorphan use from levomethorphan use, considering the possibility of the adulteration or substitution of dextromethorphan with levomethorphan for illegal purposes. However, for application to forensic toxicological purposes, further studies should be carried out using authentic human samples.

The concentrations of dextromethorphan and levomethorphan in the rat hair were obviously high compared with those of metabolites in the plasma and urine samples in this study. In our previous study [38], we determined the melanin affinity and lipophilicity of 20 abused drugs and these values were compared with the ratio of drug concentration in hair to plasma AUC as an index of the incorporation tendency into hair. As a result, the combination of melanin affinity (basicity) and lipophilicity showed a high correlation with the incorporation tendency into hair. Parent compounds can be detected relatively easily in hair in comparison with their hydrophilic metabolites. Actually, it has been reported that cocaine is detected in hair at a much higher concentration than its metabolite, benzoylecgonine, although cocaine is rapidly hydrolyzed to benzoylecgonine and disappears from plasma [39]. Considering those reports, the physico-chemical properties of dextromethorphan/levomethorphan and their metabolites could be significantly related to their concentrations in the hair samples. Additionally, the drug concentrations in the rat hair (collected 4 weeks after the first administration) reflected the total amounts of drugs in the plasma of rats administered with dextromethorphan/levomethorphan for ten successive days, and the differences might become more distinct. The detection of the parent compounds from hair samples would provide useful information regarding the monitoring of their use over a long period.

In the DA rat samples, obvious differences in the ratios of the metabolites were found between the dextro and levo forms. These differences were most clearly detected in the hair samples. The concentrations of the parent compounds, their *O*-demethyl, *N*-demethyl, and *N*, *O*-didemethyl metabolites were 63.4, 2.7, 25.1, and 0.7 ng/mg for the dextro forms and 24.5, 24.6, 2.6, and 0.5 ng/mg for the levo forms, respectively. In order to investigate the differences of their metabolic properties between dextromethorphan and levomethorphan, DA rat and human liver microsomes were studied. As a result, we have shown the enantioselective metabolism of levomethorphan, not only in DA rats but also in human liver microsomes, especially with regards to the *O*-demethylation. Because it is well-known that CYP2D6 (mainly related to *O*-demethylation of dextromethorphan) is polymorphically expressed in humans, it may be difficult to discuss the enantioselective metabolism in humans who can be classified as poor, intermediate and extensive metabolizers of dextromethorphan. In future studies, the metabolic properties of these drugs using CYP2D6 enzymes (having a variety of phenotypes) should be examined to clarify the effects of their genotypes on the enantioselective *O*-demethylation of levomethorphan observed in this study.

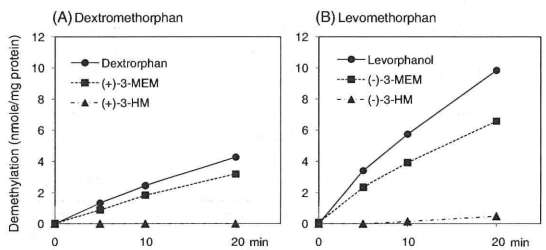

Fig. 6 Demethylation of (**A**) dextromethorphan and (**B**) levomethorphan in human liver microsomes

Conclusions

In this present study, we have established procedures for chiral analyses of dextromethorphan, levomethorphan, and their *O*-demethyl and/or *N*-demethyl metabolites in rat plasma, urine, and hair using LC-MS/MS. These analytical methods might be applied to human samples and could be useful for discriminating dextromethorphan use from levomethorphan use although further studies should be carried out using authentic human samples for forensic toxicological purposes. In addition, we have found the enantioselective metabolism of levomethorphan, not only in DA rats but also in human liver microsomes, especially with regards to the *O*-demethylation. This is the first report describing the differences in metabolic properties between dextromethorphan and levomethorphan in rats and humans.

Acknowledgments Part of this work was supported by a Health and Labor Sciences Research Grant from the Ministry of Health, Labor and Welfare in Japan.

References

1. Mutschler J, Koopmann A, Grosshans M, Hermann D, Mann K, Kiefer F (2010) Dtsch Arztebl Int 107:537–540
2. Chyka PA, Erdman AR, Manoguerra AS, Christianson G, Booze LL, Nelson LS, Woolf AD, Cobaugh DJ, Caravati EM, Scharman EJ, Troutman WG (2007) Clin Toxicol 45:662–677
3. Banken JA, Foster H (2008) Ann NY Acad Sci 1139:402–411
4. Shin EJ, Lee PH, Kim HJ, Nabeshima T, Kim HC (2008) J Pharmacol Sci 106:22–27
5. Bryner JK, Wang UK, Hui JW, Bedodo M, MacDougall C, Anderson IB (2006) Arch Pediatr Adolesc Med 160:1217–1222
6. Miller SC (2005) Addict Biol 10:325–327
7. Logan BK, Goldfogel G, Hamilton R, Kuhlman J (2009) J Anal Toxicol 33:99–103
8. Rammer L, Holmgren P, Sandler H (1988) Forensic Sci Int 37:233–236
9. Woods JW, Carney J (1978) NIDA Res Monogr 18:54–66
10. Trescot AM, Datta S, Lee M, Hansen H (2008) Pain Physician 11: S133–S153
11. Jacqz-Aigrain E, Funck-Brentano C, Cresteil T (1993) Pharmacogenetics 3:197–204
12. Schmid B, Bircher J, Preisig R, Küpfer A (1985) Clin Pharmacol Ther 38:618–624
13. Gorski JC, Jones DR, Wrighton SA, Hall SD (1994) Biochem Pharmacol 48:173–182
14. Köppel C, Tenczer J, Arndt I, Ibe K (1987) Arzneimittelforschung 37:1304–1306
15. Lutz U, Bittner N, Lutz RW, Lutz WK (2008) J Chromatogr B 871:349–356
16. Kristensen HT (1998) J Pharm Biomed Anal 18:827–838
17. Aumatell A, Wells RJ (1993) J Chromatogr Sci 31:502–508
18. Lin SY, Chen CH, Ho HO, Chen HH, Sheu MT (2007) J Chromatogr B 859:141–146
19. Bendriss EK, Markoglou N, Wainer IW (2001) J Chromatogr B 754:209–215
20. Afshar M, Rouini MR, Amini M (2004) J Chromatogr B 802:317–322
21. Hendrickson HP, Gurley BJ, Wessinger WD (2003) J Chromatogr B. B 788:261–268
22. Kim SC, Chung H, Lee SK, Park YH, Yoo YC, Yun YP (2006) Forensic Sci Int 161:185–188
23. Spanakis M, Vizirianakis IS, Mironidou-Tzouveleki M, Niopas I (2009) Biomed Chromatogr 23:1131–1137
24. Rodrigues WC, Wang G, Moore C, Agrawal A, Vincent MJ, Soares JR (2008) J Anal Toxicol 32:220–226
25. Kim EM, Lee JS, Park MJ, Choi SK, Lim MA, Chung HS (2006) Forensic Sci Int 161:198–201
26. Bagheri H, Es-haghi A, Rouini MR (2005) J Chromatogr B 818:147–157
27. Eichhold TH, McCauley-Myers DL, Khambe DA, Thompson GA, Hoke SH 2nd (2007) J Pharm Biomed Anal 43:586–600
28. Kuhlenbeck DL, Eichold TH, Hoke SH 2nd, Baker TR, Mensen R, Wehmeyer KR (2005) Eur J Mass Spectrom 11:199–208
29. Lutz U, Völkel W, Lutz RW, Lutz WK (2004) J Chromatogr B 813:217–225
30. Vengurlekar SS, Heitkamp J, McCush F, Velagaleti PR, Brisson JH, Bramer SL (2002) J Pharm Biomed Anal 30:113–124
31. Sunouchi M, Fukuhara M, Ohno Y, Takanaka A (1988) J Toxicol Sci 13:193–204
32. Ozawa S, Ohta K, Miyajima A, Kurebayashi H, Sunouchi M, Shimizu M, Murayama N, Matsumoto Y, Fukuoka M, Ohno Y (2000) Xenobiotica 10:1005–1017
33. Kikura-Hanajiri R, Kawamura M, Saisho K, Kodama Y, Goda Y (2007) J Chromatogr B 855:121–126
34. Kikura-Hanajiri R, Kawamura M, Miyajima A, Sunouchi M, Goda Y (2010) Forensic Sci Int 198:62–69
35. Bochner F, Somogyi AA, Chen ZR (1994) Xenobiotica 24:543–552
36. Kerry NL, Somogyi AA, Mikus G, Bochner F (1993) Biochem Pharmacol 45:833–839
37. Zysset T, Zeugin T, Küpfer A (1988) Biochem Pharmacol 37:3155–3160
38. Nakahara Y, Takahashi K, Kikura R (1995) Biol Pharm Bull 18:1223–1227
39. Nakahara Y, Ochiai T, Kikura R (1992) Arch Toxicol 66:446–449

Molecular Responses of Human Lung Epithelial Cells to the Toxicity of Copper Oxide Nanoparticles Inferred from Whole Genome Expression Analysis

Nobutaka Hanagata,[†,‡,*] Fei Zhuang,[‡,§] Sarah Connolly,[†,∥] Jie Li,[†] Nobuhiro Ogawa,[§] and Mingsheng Xu[⊥]

[†]Nanotechnology Innovation Station, National Institute for Materials Science, 1-2-1 Sengen, Tsukuba, Ibaraki 305-0047, Japan, [‡]Graduate School of Life Science, Hokkaido University, N10W8, Kita-ku, Sapporo 060-0812, Japan, [§]Biomaterials Unit, National Institute for Materials Science, 1-2-1 Sengen, Tsukuba, Ibaraki 305-0047, Japan, and [⊥]State Key Laboratory of Silicon Materials, MOE Key Laboratory of Macromolecule Synthesis and Functionalization, and Department of Polymer Science and Engineering, Zhejiang University, Hangzhou 310027, People's Republic of China. [∥]Present address: Microbiology and Cell Science, University of Florida, Gainesville, Florida 32611-0700.

ABSTRACT This study proposes a molecular mechanism for lung epithelial A549 cell response to copper oxide nanoparticles (CuO-NPs) related to Cu ions released from CuO-NPs. Cells that survived exposure to CuO-NPs arrested the cell cycle as a result of the downregulation of proliferating cell nuclear antigen (PCNA), cell division control 2 (CDC2), cydin B1 (CCNB1), target protein for Xklp2 (TPX2), and aurora kinase A (AURKA) and B (AURKB). Furthermore, cell death was avoided through the induced expression of nuclear receptors NR4A1 and NR4A3 and growth arrest and DNA damage-inducible 45 β and γ (GADD45B and GADD45G, respectively). The downregulation of CDC2, CCNB1, TPX2, AURKA, and AURKB, the expressions of which are involved in cell cycle arrest, was attributed to Cu ions released from CuO-NPs into medium. NR4A1 and NR4A3 expression was also induced by Cu ions released into the medium. The expression of GADD45B and GADD45G activated the p38 pathway that was involved in escape from cell death. The upregulation of GADD45B and GADD45G was not observed with Cu ions released into medium but was observed in cells exposed to CuO-NPs. However, because the expression of the genes was also induced by Cu ion concentrations higher than that released from CuO-NPs into the medium, the expression appeared to be triggered by Cu ions released from CuO-NPs taken up into cells. We infer that, for cells exposed to CuO-NPs, those able to make such a molecular response survived and those unable to do so eventually died.

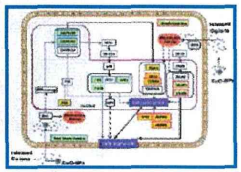

KEYWORDS: copper oxide nanoparticles · cytotoxicity · lung epithelial cells · cell cycle arrest · DNA microarray

As a result of recent advances in nanotechnology, the industrial use of nanomaterials is increasing. Although the size, shape, surface area, and surface activity of nanomaterials are attractive for many different applications, concern exists that these properties may contribute to the toxicity of nanomaterials. For example, their small size could allow them to easily enter the body through respiratory passages or wounds and affect various tissues. However, clear safety standards have not been established for nanomaterials.

Previously, we demonstrated that copper oxide nanoparticles (CuO-NPs) are the most toxic metal oxide nanoparticles.[1,2] CuO-NPs are used in textiles for their antibacterial effects.[3] They are also being developed for use in catalysts, gas sensors, microelectronic materials, and cosmetics.[4,5] Furthermore, Cu-NPs are added as materials to ink, plastics, lubricants, metallurgical coatings, and cosmetics for the skin.[6] Although SiO_2-NPs (15–25 nm), CeO_2-NPs (20 nm), and Al_2O_3-NPs (15–50 nm) are not toxic to A549 cells, ZnO-NPs (20–60 nm) are cytotoxic to a lesser extent than CuO-NPs.[1,2]

These findings suggest that the toxicity of metal oxide nanoparticles is not due to their size but their chemical composition. Specifically, metal oxide nanoparticles such as CuO-NPs and ZnO-NPs that release metal ions are most likely to be cytotoxic. In addition to CuO-NPs and ZnO-NPs, Ag-NPs are highly cytotoxic to HeLa cervical cancer cells, and Ag ions that are released into the culture medium are responsible for much of the toxicity.[7] However, until recently, the nanoparticles themselves, rather than released Cu ions, have been suggested to cause CuO-NP cytotoxicity.[8,9] The uptake of CuO-NPs into cells and subsequent generation of intracellular reactive oxygen species (ROS) have been reported to cause cytotoxicity and genotoxicity,[8,10] but the molecular basis of CuO-NP toxicity has not been clarified.

* Address correspondence to hanagata.nobutaka@nims.go.jp.

Received for review May 10, 2011 and accepted November 11, 2011.

Published online November 11, 2011
10.1021/nn202966t

Human lung epithelial A549 cells were used in this study because we have a greater chance of inhaling nanoparticles in the workplace rather than taking them up through the skin, ingestion, and injection. A549 cells that were derived from carcinoma tissue are classified as type I pneumocytes, which cover >95% of the internal surface that provides a barrier function and gas exchange in the lung. We used DNA microarrays to analyze the effects of CuO-NPs on the global gene expression of A549 cells. First, we identified genes affected by exposure to CuO-NPs and inferred functional changes of cells using gene ontology (GO) analysis, in which affected genes were classified into functional categories. Next, we performed global gene expression analysis of cells exposed to Cu ions released from CuO-NPs into medium and identified genes that were regulated by both CuO-NPs and released Cu ions. These analyses revealed the contribution of released Cu ions to the toxicity of CuO-NPs at the molecular level. Furthermore, we examined the gene expression of cells exposed to different concentrations of $CuCl_2$ to confirm the contribution of Cu ions released from CuO-NPs. Our results suggest that the *in vitro* cytotoxicity of CuO-NPs is primarily due to the effects of Cu ions that are released into the culture medium and absorbed into cells.

RESULTS AND DISCUSSION

Preparation and Characterization of Medium Containing Cu Ions Released from CuO-NPs. The average diameter of CuO-NPs used in this study was 50 nm,[1] and the mean aggregate size of the particles after dispersal in medium at a concentration of 25 μg/mL was around 300 nm (Supporting Information Figure S1). However, CuO-NPs were immediately sedimented. The morphology and electronic properties of CuO-NPs have been reported previously.[1]

To investigate the contribution of the released Cu ions to the toxicity of CuO-NPs, we prepared culture medium containing Cu ions released from CuO-NPs (Supporting Information Figure S2a). CuO-NPs (25 μg/mL final concentration) were added to the culture medium and incubated at 37 °C for 24 h. Then, the medium containing CuO-NPs was centrifuged at 150 000*g* for 1 h to remove the CuO-NPs. Inductively coupled plasma optical emission spectrometry (ICP-OES) indicated that the Cu concentration in the resulting supernatant was 13.2 ± 1.54 μg/mL (11.6–15.0 μg/mL, $n = 5$). To examine the presence or absence of CuO-NPs in the supernatant, we analyzed the supernatant using a laser diffraction particle analyzer (DLS). The analysis revealed the presence of NPs in the supernatant (Figure 1a). However, the similar pattern of size distribution was also observed in the culture medium without CuO-NPs after incubation at 37 °C for 24 h (Figure 1b and Supporting Information Figure S2b), suggesting that the NPs in the supernatant are attributed to medium components, not CuO-NPs. In addition, as shown by transmission electron microscopy (TEM) and energy-dispersive spectroscopy (EDS) (Figure 1c–f), NPs in the supernatant contained hardly any CuO-NPs. On the other hand, observation of the resulting precipitation that contains CuO-NPs removed from the culture medium, using scanning electron microscope (SEM), revealed CuO-NPs with smaller than original size (Figure 1g,h). This implies that CuO-NPs released Cu ions into the culture medium, resulting in smaller size. Therefore, we used the supernatant as the culture medium containing released Cu ions to assess the contribution of the released Cu ions to the toxicity of CuO-NPs. Although CuO-NPs released Cu ions into the medium, they hardly released the ions in water (Supporting Information Figure S2c).

Toxicity of CuO-NPs. The number of viable A549 cells cultured in 25 μg/mL CuO-NPs or the supernatant was 34 and 81% of that of the control culture, respectively (Figure 2a and Supporting Information Figure S3). This result indicated that released Cu ions are also toxic and may account for part of the toxicity of CuO-NPs. In addition, we used the water-soluble tetrazolium salt (WST) cell proliferation assay, which is based on the production of formazan from WST-8 by mitochondrial dehydrogenases in viable cells, to measure cytotoxicity. The amount of formazan produced by cells cultured in 25 μg/mL CuO-NPs or the supernatant was 20 and 57% of that of the control culture, respectively (Figure 2b). This result implies that the CuO-NPs and released Cu ions damaged the mitochondria. This damage occurred after 4 h of exposure to CuO-NPs (Supporting Information Figure S4). Furthermore, supplementation of Al_2O_3-NPs with 50 nm in size that were used as nontoxic dummy NPs to the supernatant did not affect the formazan formation of the supernatant (Supporting Information Figure S5), suggesting released Cu ions alone damaged mitochondria. Approximately 9% of cells underwent apoptosis in response to CuO-NPs, but we observed few apoptotic cells in culture with the supernatant (Figure 2c). These results suggested that CuO-NPs damaged mitochondria and induced apoptosis, and that released Cu ions were responsible for some of the damage to the mitochondria.

To confirm the contribution of released Cu ions to the toxicity of CuO-NPs, we examined the cytotoxicity of different concentrations of $CuCl_2$. In cultures with the supernatant, the number of viable cells and the amount of formazan was 81 and 57% of control culture levels (Figure 2a,b). The concentration of $CuCl_2$ required for similar toxicity was 25–33 μg/mL (Figure 2d,e). This concentration is equivalent to 11.8–15.6 μg/mL Cu ions, which was consistent with the concentration of Cu ions that were released from CuO-NPs. This result showed that the effect of Cu ions that are released from CuO-NPs is similar to that of Cu ions from $CuCl_2$.

Next, we examined the uptake of CuO-NPs into cells using TEM. NP-like structures were observed inside cell (Supporting Information Figure S6). To verify whether

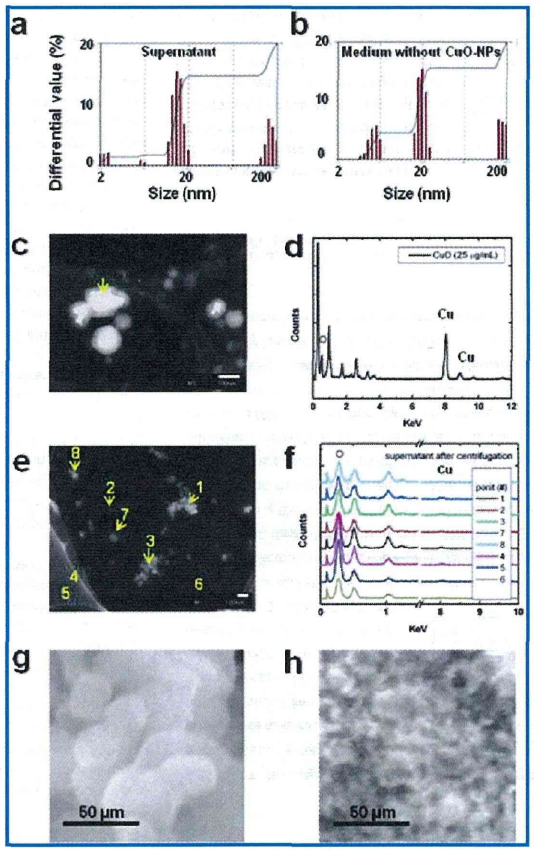

Figure 1. Characterization of supernatant for preparation of medium containing Cu ions released from CuO-NPs. (a) Size distribution of NPs in supernatant. (b) Size distribution of NPs in medium without CuO-NPs incubated at 37 °C for 24 h. (c) Dark-field TEM image of a CuO-NP sample. A TEM grid was immersed into the cell culture medium that contained 25 μg/mL CuO-NPs and then air-dried. (d) EDS spectrum of the point indicated by the arrow in (c), which suggests the presence of Cu and O. (e) Dark-field TEM image of the supernatant. The CuO-NP suspension was centrifuged at 150 000g for 1 h. Subsequently, a TEM grid was immersed into the supernatant and then air-dried. (f) EDS spectra of points 1−8 in (e). (g) SEM image of original CuO-NPs. (h) SEM image of CuO-NPs incubated in medium at 37 °C for 24 h.

these NP-like structures are attributed to CuO-NPs, elemental maps were analyzed. The elemental maps clearly showed that CuO-NPs were taken up into cell (Figure 3).

Molecular Response of Cells to CuO-NPs. To elucidate the underlying molecular mechanism of CuO-NP toxicity, comprehensive gene expression analysis was performed using DNA microarray. We exposed A549 cells to 25 μg/mL CuO-NPs for 24 h and then identified genes that demonstrated greater than 2-fold change in expression level compared with those in control cells. Our results revealed that CuO-NPs upregulated the expression of 648 genes and downregulated the expression of 562 genes. These data have been deposited in the Gene Expression Omnibus database with accession code GE33278. By classifying these genes into GO functional categories, we obtained the following statistically significant categories ($p < 0.001$): CuO-NPs upregulated genes

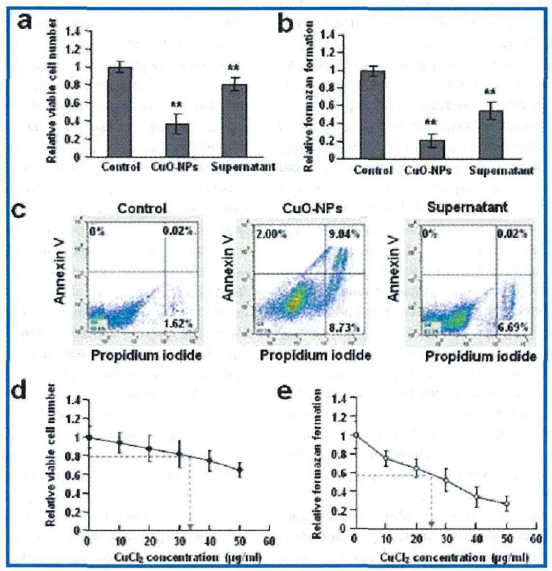

Figure 2. Toxicity of CuO-NPs and released Cu ions. (a) Cytotoxicity of CuO-NPs and supernatant as indicated by the number of viable cells. A549 human lung epithelial cells were cultured in media containing 25 μg/mL CuO-NPs or supernatant at 37 °C for 24 h, and then the number of viable cells was compared to that of control (untreated) cells (defined as 1). Results are expressed as mean (SE) ($n = 4$); $^{**}p < 0.05$. (b) Cytotoxicity of CuO-NPs and supernatant as indicated by cell viability in the WST assay. Results are expressed as mean (SE) ($n = 8$); $^{**}p < 0.05$. (c) Ratio of apoptotic cells determined by using flow cytometry. Cells were stained with propidium iodide and FITC-labeled Annexin V; 20 000 cells were analyzed. Apoptotic cells are distributed in the upper right-hand area. Apoptosis was not observed in cells exposed to supernatant. However, about 9% of cells underwent apoptosis in response to CuO-NPs. Living cells in early apoptotic stage are distributed in the upper left-hand area. Therefore, only 2% of cells were in the early apoptotic stage when cells were exposed to CuO-NPs. (d) Cytotoxicity of $CuCl_2$ as indicated by the number of viable cells. Arrow indicates concentration of $CuCl_2$ whose toxicity is similar to that of supernatant. (e) Cytotoxicity of $CuCl_2$ as indicated by cell viability. Arrow indicates concentration of $CuCl_2$ whose toxicity is similar to that of supernatant.

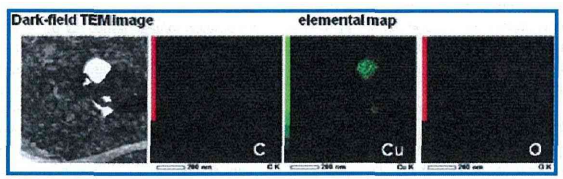

Figure 3. Dark-field TEM image and elemental map of NPs inside cells. A549 cells were cultured in medium containing 25 μg/mL CuO-NPs at 37 °C for 24 h, and then living cells were harvested for the observation. Elemental map suggests the presence of Cu and O.

that affect "nucleobase, nucleoside, nucleotide, and nucleic acid metabolic processes" and "response to stress" and downregulated genes that affect "cell cycle", "mitosis", "cytokinesis", "chromosome segregation", "cellular component organization", and "cellular component morphogenesis" (Figure 4; a list of genes in each category is shown in Supporting Information Tables S1−S6). The upregulated 31 genes in the response to stress category included genes that encode heat shock proteins (HSPs) (Supporting Information Table S2) and proteins involved in mitogen-activated protein kinase (MAPK) pathways, such as growth arrest and DNA damage-inducible 45 β and γ (GADD45B/GADD45G) and nuclear receptors 4A1 and 3 (NR4A1/NR4A3) (Figure 4a and Table 1).

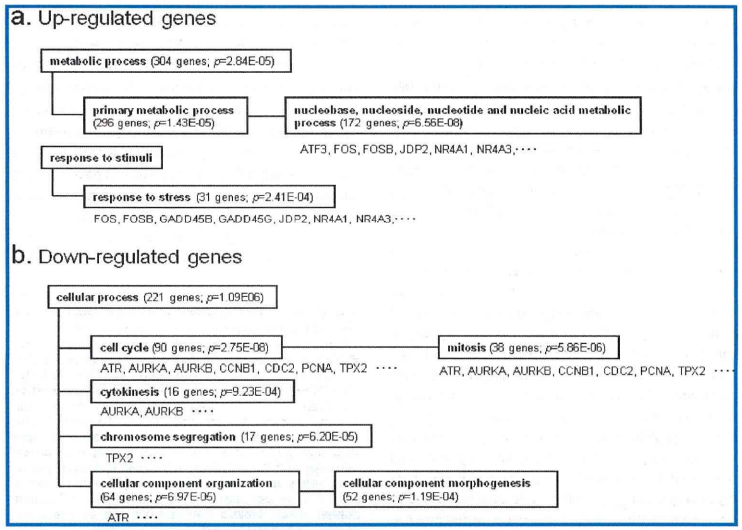

Figure 4. Gene ontology classification of genes that were upregulated or downregulated by CuO-NPs. A549 cells were exposed to 25 μg/mL CuO-NPs for 24 h, and then DNA microarray analysis was used to identify genes that demonstrated a 2-fold or greater change in expression level compared with control cells. These genes were grouped into statistically significant GO functional categories ($p < 0.001$). (a) Functional categories of genes upregulated by CuO-NPs. The numbers within parentheses indicate the number of genes in each category. (b) Functional categories of genes downregulated by CuO-NPs. Representative genes are shown in each category. The gene list for each category is included in Supporting Information (Tables S1–S6).

We confirmed the upregulation of GADD45B/GADD45G and NR4A1/NR4A3 at protein level by using Western blot analysis (Supporting Information Figure S7).

The upregulation of many HSPs suggested that CuO-NPs stimulate protein denaturation. GADD45B and GADD45G are members of the GADD45 family of proteins that are induced by genotoxic stresses and various apoptotic cytokines[11–13] and are involved in cell cycle arrest,[14–19] DNA repair,[20–22] cell survival,[22–27] and apoptosis.[28–37] These functions are mediated by proliferating cell nuclear antigen (PCNA), cell division control 2 (CDC2), cyclin B1 (CCNB1), and cyclin-dependent kinase inhibitor 1A (CDKN1A; also known as p21), which are classified in the GO cell cycle category. PCNA is involved in DNA repair and the transition from the G1 to the S phase of the cell cycle.[20–22] In contrast, CDKN1A inhibits PCNA and blocks the transition from the G1 to the S phase of the cell cycle.[20,38] The CDC2–CCNB1 complex is required for the transition from the G2 to the M phase.[39,40] Although CuO-NPs did not affect the expression of CDKN1A, they downregulated the expression of PCNA, CDC2, and CCNB1 (Figure 4b and Table 1), which suggests that CuO-NPs induce cell cycle arrest in the G1 and G2 phases. In addition, CuO-NPs downregulated the expression of genes that encode aurora kinase A and B (AURKA/AURKB) and target protein for XKlp2 (TPX2) (Figure 4b and Table 1), which peak during the G2/M transition and are involved in the assembly and maintenance of the spindle.[41]

To confirm that CuO-NPs cause cell cycle arrest, we isolated cells that survived exposure to CuO-NPs and cultured them in fresh culture medium that did not contain CuO-NPs. However, these cells did not proliferate for 72 h (Supporting Information Figure S8a). When we harvested these cells and cultured them again in fresh culture medium that did not include CuO-NPs for an additional 72 h, their proliferative capacity was restored; however, their rate of proliferation lagged behind that of control cells (Supporting Information Figure S8b). These results indicated that the surviving cells were in a state of cell cycle arrest after exposure to CuO-NPs. Since cell cycle arrest is thought to provide time for cells to repair damaged DNA, it is likely that CuO-NPs compromise cell survival.

The expression of GADD45B and GADD45G has been reported to activate the c-Jun N-terminal kinase (JNK) and p38 pathways *via* MAP 3 kinase 1 (MTK1).[28,42,43] In addition, activation of these pathways

TABLE 1. Fold Change of Gene Expression Level Mainly Discussed in This Study

	fold-change (log_2 ratio)[a]						
	CuO-NP (25 μg/mL)		supernatant (contained about 15 μg Cu/mL)		$CuCl_2$ (30 μg/mL)	$CuCl_2$ (60 μg/mL)	
gene name	DNA microarray	qPCR	DNA microarray	qPCR	qPCR	qPCR	GO category
GADD45A	0.24	0.55	−0.76	0.68	0.14	1.07	response to stress
GADD45B	2.96	3.00	−0.02	0.30	−0.42	1.52	response to stress
GADD45G	3.59	3.22	NR	0.61	0.38	1.70	response to stress
PCNA	−1.37	−0.87	NR	−0.28	−0.05	−0.23	cell cycle
CDC2	−1.41	−1.48	−1.16	−1.08	−1.40	−1.22	cell cycle
CCNB1	−1.74	−2.14	−1.33	−1.51	−1.27	−1.46	cell cycle
CDKN1A	0.30	0.78	−0.08	0.63	−0.07	−0.49	cell cycle
FOS	4.48	1.06	NR	−0.14	0.37	0.61	nucleobase, nucleoside, nucleotide and nucleic acid metabolic process; response to stress
FOSB	5.70	3.97	NR	0.68	0.57	3.43	nucleobase, nucleoside, nucleotide and nucleic acid metabolic process; response to stress
ATF3	4.22	1.23	NR	−0.01	0.07	1.14	nucleobase, nucleoside, nucleotide and nucleic acid metabolic process
JDP2	1.13	−0.67	NR	−0.19	−0.36	−0.41	nucleobase, nucleoside, nucleotide and nucleic acid metabolic process
ATR	−1.11	−0.83	−0.20	−0.48	−0.33	−0.51	cell cycle; cellular component organization
TP53	NR	−1.10	NR	−1.12	−0.04	0.15	induction of apoptosis; cell cycle; Nucleobase, nucleoside, nucleotide and nucleic acid metabolic process
NR4A1	5.28	2.82	2.71	1.25	0.89	2.09	nucleobase, nucleoside, nucleotide and nucleic acid metabolic process; response to stress
NR4A2	NR	−1.12	NR	−0.96	0.07	0.33	nucleobase, nucleoside, nucleotide and nucleic acid metabolic process; response to stress
NR4A3	3.06	1.08	NR	0.94	1.55	2.96	nucleobase, nucleoside, nucleotide and nucleic acid metabolic process; response to stress
AURKA	−1.21	−1.62	−0.91	−1.34	−0.59	−1.12	cell cycle; cytokinesis
AURKB	−1.13	−1.76	−0.81	−1.18	−0.96	−1.37	cell cycle; cytokinesis
TPX2	−1.25	−2.13	−1.17	−1.63	−1.16	−2.11	cell cycle; chromosome segregation

[a] Fold-change is represented by logarithmic ratio (log_2 ratio) to expression level in control. NR: Not reproducible.

induces the activation of the constituent proteins of the activator protein 1 (AP-1) transcription factor complex, such as c-Jun, JunD, and activating transcription factor 2 (ATF2).[44,45] AP-1 is involved in both apoptosis and cell survival.[46,47] To examine how the JNK or p38 pathway is involved in the molecular response to CuO-NP exposure, we treated cells with CuO-NPs and either a JNK interacting protein 1 (JIP-1) peptide or SB239063, which are inhibitors of JNK and p38, respectively. Although the JIP-1 peptide did not have any effect on the number of viable cells, SB239063 markedly reduced the number of viable cells relative to treatment with CuO-NPs alone (Figure 5a and Supporting Information Figure S9). Similar to SB239063, when GADD45B in cells exposed to CuO-NPs was knocked down with small interfering RNA (siRNA) (Supporting Information Figure S10), they were more sensitive to CuO-NPs than cells with normal GADD45B expression, and the number of viable cells decreased (Figure 5b and Supporting Information Figure S11). Together, these results suggest that the upregulation of GADD45B/GADD45G due to CuO-NPs promotes cell survival by activating the p38 pathway. The activation of the p38 pathway in turn activates ATF2, which interacts with FOS, FOSB, and ATF3 in the AP-1 complex. In addition, we observed the upregulation of these proteins by CuO-NPs (Figure 4a and Table 1), which strongly suggested that the underlying mechanism of cell survival involved the p38 pathway.

CuO-NPs also upregulated NR4A1 and NR4A3. These nuclear receptors are involved in both cell survival and apoptosis and are activated *via* the mitogen-activated protein kinase/extracellular signal-regulated kinase 5 (MEK5/ERK5) pathways.[48,49] When NR4A1 in cells exposed to CuO-NPs was knocked down with siRNA (Supporting Information Figure S10), A549 cells were more sensitive to CuO-NPs than cells with normal NR4A1 expression, and the number of viable cells decreased (Figure 5b and Supporting Information Figure S11). These results indicated that the upregulation of NR4A1 is also involved in cell survival after exposure to CuO-NPs.

DNA damage is well-known to activate p53, which induces checkpoint arrest in the G1 and G2/M phases of the cell cycle and apoptosis in cells that cannot recover from DNA damage.[50] The checkpoint function of p53 is activated by the phosphorylation of ataxia telangiectasia mutated (ATM), ataxia telangiectasia and Rad3-related protein (ATR), and checkpoint kinase

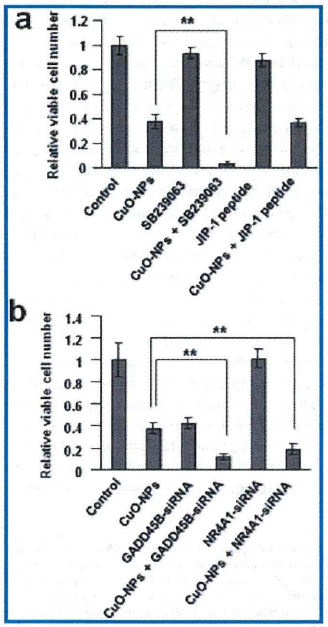

Figure 5. Changes in the number of viable cells due to disruption of mitogen-activated protein kinase (MAPK) pathways. After culturing A549 cells for 42 h, p38 or c-Jun N-terminal kinase (JNK) inhibitors or siRNA were added and incubated for 6 h. Subsequently, CuO-NPs were added to a final concentration of 25 μg/mL and then cultured for 24 h. (a) Effects of SB239063 and JNK interacting protein 1 (JIP-1), which are inhibitors of p38 and JNK, respectively, on the number of viable cells. SB239063 increased the cytotoxicity of CuO-NPs ($n = 3$); $^{**}p < 0.05$. (b) Effect of siRNA knockdown on the expression of GADD45B and NR4A1 on the cytotoxicity of CuO-NPs. Knockdown of the expression of these genes markedly increased the cytotoxicity of CuO-NPs ($n = 3$); $^{**}p < 0.05$. The knockdown efficiency for each gene is shown in Supporting Information Figure S10.

1 (Chk1). Subsequently, activated p53 induces the expression of GADD45A and CDKN1A.[30,51−54] Although CuO-NPs downregulated ATR, they did not affect the expression of GADD45A or CDKN1A (Table 1). Therefore, we concluded that p53 does not play a major role in the response of cells exposed to CuO-NPs.

Contribution of Cu Ions Released from CuO-NPs at the Molecular Level. In addition to the genes that demonstrated altered expression in response to CuO-NPs, we identified genes that were altered in response to the Cu ions released from CuO-NPs into culture medium to determine their contribution to the molecular response to CuO-NP exposure. Cells exposed to the supernatant for 24 h upregulated 108 genes (Figure 6a). Of these 108 genes, 54 were also found in the list of 648 genes upregulated by CuO-NPs (Figure 6a and Supporting Information Table S7). Therefore, of 648 genes upregulated by CuO-NPs, 594 upregulated genes were induced by CuO-NPs themselves, but 54 upregulated genes were attributable to Cu ions released from CuO-NPs into the culture medium. After classifying these 54 shared genes into GO functional categories, we did not identify any statistically significantly enriched categories. This finding suggests that released Cu ions do not contribute to changes in cellular functions related to nucleobase, nucleoside, nucleotide, and nucleic acid metabolic processes or response to stress, categories found to be enriched in the classification of genes upregulated by CuO-NPs. The changes in these two functions were specifically induced by CuO-NPs themselves. However, NR4A1 and NR4A3, which are involved in response to stress, were upregulated by both CuO-NPs and the supernatant (Table 1 and Supporting Information Table S7), suggesting that these genes were induced by Cu ions released from the CuO-NPs.

We identified genes encoding super oxide dismutase 2 (SOD2), which functions as a ROS quencher, and 9 genes for metallothionein isomers (MT1A, MT1B, MT1E, MT1F, MT1G, MT1H, MT1L, MT1X, and MT2A) among the 54 common genes upregulated by both CuO-NPs and the supernatant (Figure 6a and Supporting Information Table S7). Since MT isomers help protect cells from oxidative stress due to excess metal ions, such as cadmium, zinc, and copper,[55−58] the released Cu ions may generate ROS. To examine whether CuO-NPs and Cu ions induce ROS in A549 cells, we pretreated cells with *N*-acetylcysteine (NAC), which is a ROS scavenger. NAC protected cells exposed to supernatant from mitochondrial damage (Figure 7a). NAC also partially protected cells exposed to CuO-NPs from mitochondrial damage and cell death (Figure 7b). These findings imply that ROS generation by Cu ions released from CuO-NPs is one of the causes of CuO-NP toxicity.

The supernatant also downregulated 125 genes (Figure 6b). Of these genes, 55 genes were also among the 562 genes downregulated by CuO-NPs (Figure 6b and Supporting Information Table S8). Therefore, of 562 genes downregulated by CuO-NPs, 507 genes were specifically downregulated by CuO-NPs themselves, but 55 genes were downregulated by Cu ions released from CuO-NPs. After classifying these 55 shared downregulated genes into GO categories, we identified statistically significantly enriched functional categories including cell cycle, mitosis, and chromosome segregation (Figure 6c; a list of genes in each category is shown in Supporting Information Table S9). These categories were also identified in the classification of

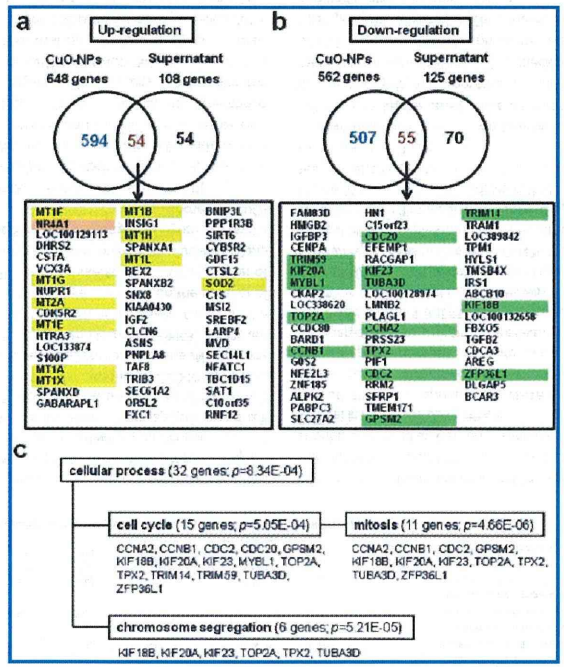

Figure 6. Gene expression altered by both CuO-NPs and released Cu ions. (a) Genes upregulated by both CuO-NPs and supernatant. Of 108 genes that were upregulated in response to supernatant, 54 genes were also upregulated by CuO-NPs. (b) Genes downregulated by both CuO-NPs and supernatant. Of 125 genes that were downregulated in response to supernatant, 55 genes were also downregulated by CuO-NPs. The names of the common genes are boxed. Yellow, orange, and green highlighting of gene names indicate ROS scavenger genes, MAPK-related gene, and cell cycle-related genes, respectively. (c) Gene ontology classification of genes that were downregulated by both CuO-NPs and supernatant. Categories with $p < 0.001$ were considered statistically significant functional categories. The numbers within parentheses indicate the number of genes in each category. Gene names are listed under each category.

genes downregulated by CuO-NPs (Figure 4b), suggesting that changes in these cellular functions by CuO-NPs were attributable to Cu ions released from CuO-NPs into culture medium.

Among genes downregulated by CuO-NPs, CDC2, CCNB1, PCNA, AURKA/AURKB, and TPX2 were classified into GO categories cell cycle, mitosis, or chromosome segregation (Figure 4b). Downregulation of CDC2, CCNB1, AURKA/AURKB, and TPX2 has been reported to induce cell cycle arrest in the G2 phase,[39−41] and downregulation of PCNA led to cell cycle arrest in the G1 phase.[20,38] Among these genes, CDC2, CCNB1, AURKA/AURKB, and TPX2 were also downregulated by the supernatant, but PCNA was not changed by the supernatant (Table 1). We observed a marked increase in the number of cells in the G2/M phase upon exposure to CuO-NPs and the supernatant compared with control cells (Figure 8). In addition, an increase in the G1 population accompanied by a decrease in the S phase population was observed in the cells exposed to CuO-NPs compared to the cells exposed to the supernatant (Figure 8). Therefore, released Cu ions are responsible for the cell cycle arrest in the G2 phase induced by CuO-NPs, while cell cycle arrest in the G1 phase is attributable to CuO-NPs themselves. This observation corresponds to the results of gene expression analysis.

A question remains: what causes the toxicity of CuO-NPs themselves? One possibility is the effect of Cu ions released from CuO-NPs taken up into cells. When Cu ions are released from internalized CuO-NPs, the intracellular concentration of Cu ions increases. Indeed, in cells cultured in medium containing 60 μg/mL $CuCl_2$, which has a Cu ion concentration twice of that

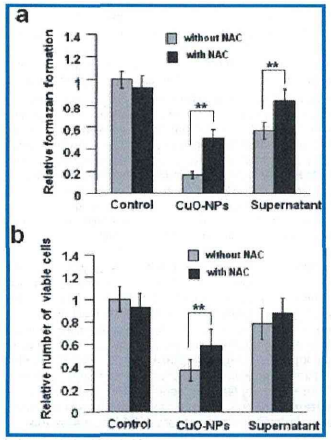

Figure 7. Effect of pretreatment of cells with NAC, a scavenger of ROS. (a) NAC decreased mitochondrial damage of cells exposed to CuO-NPs and supernatant (n = 8); **p < 0.05. (b) NAC increased the number of living cells exposed to CuO-NPs and supernatant (n = 3); **p < 0.05.

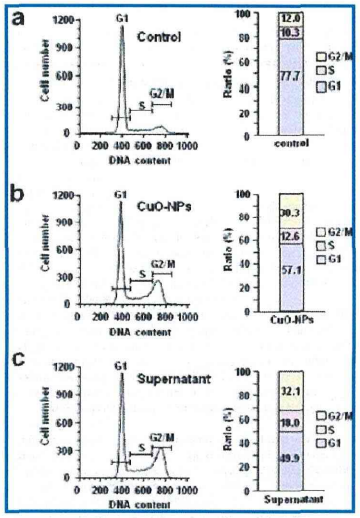

Figure 8. Cell cycle analysis in A549 cells determined by flow cytometry. A549 cells cells were cultured for 48 h and then were exposed to CuO-NPs and supernatant for another 24 h. Viable cells were harvested and stained with PI. (a) Control cells. These cells were under confluent. (b) Cells exposed to 25 μg/mL CuO-NPs for 24 h. (c) Cells exposed to supernatant for 24 h.

released from CuO-NPs into culture medium, the expression levels of GADD45B, GADD45G, FOSB, and ATF3, which were induced by CuO-NPs but not Cu ions released from CuO-NPs into culture medium, were upregulated (Table 1). These results suggest that the changes in gene expression due to CuO-NP exposure might not be due to the nanoparticles themselves but rather to the high concentration of Cu ions that are released from internalized CuO-NPs.

Proposed Mechanism for Cellular Response to CuO-NPs. We propose a model for cellular responses to the toxicity of CuO-NPs on the basis of these results (Figure 9). In this model, CuO-NPs damage both mitochondria and DNA, and Cu ions that are released into the culture medium contribute to the mitochondrial damage. In addition, released Cu ions generate ROS and lead to cell cycle arrest at the G2 phase by altering the expression of various cell cycle genes such as CDC2, CCNB1, TPX2, AURKA, and AURKB. Moreover, CuO-NPs induce the expression of many HSPs and strongly arrest the cell cycle at the G1 phase by downregulating PCNA. Furthermore, cells that are exposed to CuO-NPs avoid cell death by activating the p38 pathway *via* upregulation of GADD45B and GADD45G. We observed numerous CuO-NPs in dead cells compared to viable cells (Supporting Information Figure S12), suggesting that the difference in the amount of CuO-NPs that are absorbed into individual cells may determine their fate.

Finally, we examined toxicity of CuO-NPs using primary human lung epithelial cells. CuO-NPs and Cu ions also showed a toxic effect on primary cells (Supporting Information Figure S13). In addition, primary cells upregulated expression of genes involved in MAPK pathways such as GADD45B/GADD45G and NR4A1/NR4A3, which is similar to that in A549 cells (Supporting Inofrmation Figure S13). However, expression of several genes related to cell cycle regulation such as PCNA, CDC2, and AURKB showed a different pattern from that of A549 cells.

This study demonstrated that change of gene expression in A549 cells exposed to CuO-NPs is similar to that of cells exposed to $CuCl_2$, which suggests that Cu ions that are released from CuO-NPs inside and outside cells may be the primary cause of their cytotoxicity. However, our model established using A549 cells does not completely explain the molecular responses to the toxic effects of CuO-NPs. For example, although CuO-NPs downregulated PCNA, a high concentration of $CuCl_2$ did not have a similar effect. In addition, our model does not entirely apply to primary human lung epithelial cells because some of genes showed different expression patterns from that of A549 cells. Further studies are needed to elucidate the differences in molecular mechanism of primary cells from that of A549 cells demonstrated in this study.

CONCLUSIONS

CuO-NPs showed strong cytotoxicity to carcinoma-derived human lung epithelial A549 cells *in vitro*.

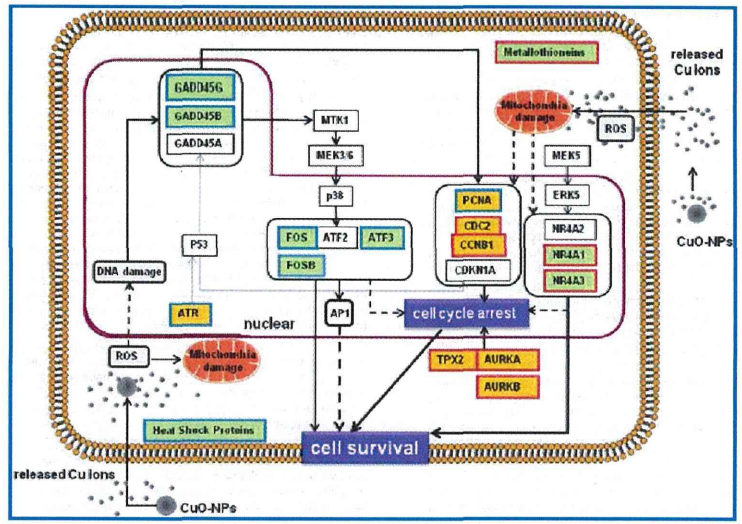

Figure 9. Model of the molecular responses of cells exposed to CuO-NPs. The boxes outlined in blue and red indicate genes that are induced by CuO-NPs and released Cu ions, respectively. Orange and light green boxes indicate downregulated and upregulated genes, respectively. The solid black lines indicate pathways that are induced by CuO-NPs or released Cu ions, while the dotted lines indicate inferred pathways. The gray lines indicate pathways that are not induced by CuO-NPs. Cells that survive exposure to CuO-NPs halt their cell cycle progression *via* downregulation of PCNA, CDC2, CCNB1, tTPX2, AURKA, and AURKB. Cell death is also prevented by the induction of NR4A1, NR4A3, GADD45B, and GADD45G. In addition, Cu ions that are released into the culture medium downregulate CDC2, CCNB1, TPX2, AURKA, and AURKB and upregulate NR4A1 and NR4A3. However, the expression of PCNA is only downregulated by CuO-NPs. The expression of GADD45B and GADD45G activates the p38 pathway to prevent cell death. Furthermore, CuO-NPs upregulate the expression of FOS, FOSB, and ATF3. These products dimerize with ATF2, which is activated by the p38 pathway, to form the AP-1 transcription factor complex. It is not known whether activation of the p38 pathway and upregulation of NR4A1/NR4A3 are involved in cell survival *via* cell cycle arrest. The induced expression of GADD45B and GADD45G is thought to be due to the absorption of Cu ions that are released from CuO-NPs into cells.

CuO-NPs upregulated genes involved in MAPK pathways such as GADD45B/GADD45G and NR4A1/NR4A3, while downregulated genes involved in cell cycle progression. Of these changes in gene expression, upregulation of NR4A1/NR4A3 and downregulation of genes related to cell cycle progression were attributed to Cu ions released from CuO-NPs into culture medium. Although GADD45B/GADD45G were not induced by Cu ions released into culture medium, higher concentration of Cu ions prepared from $CuCl_2$ enhanced the expression. The results indicated that change of gene expression involved in MAPK pathways and cell cycle progression in cells exposed to CuO-NPs was similar to that in cells exposed to Cu ions.

MATERIALS AND METHODS

CuO Nanoparticles. CuO nanoparticles (CuO-NPs) were purchased from Sigma-Aldrich (MO, USA). The average diameter of these particles was 50 nm. The mean aggregate size of the particles after dispersal in a medium was assessed using a laser diffraction particle size analyzer (DLS6000AL, Otsuka, Japan) at a concentration of 25 μg/mL.

Preparation of Medium Containing CuO-NPs and Medium Containing Released Cu Ions. To prepare the medium containing CuO-NPs, CuO-NPs were first dispersed in water sterilized with ultrasonic waves for 15 min. Next, CuO-NPs were added to high-glucose Dulbecco's modified Eagle's medium supplemented with 10% fetal bovine serum, 100 units/mL penicillin, and 100 μg/mL streptomycin (hereafter referred to as DMEM) to obtain a concentration of 25 μg/mL CuO-NPs. This medium was prepared just prior to its use. To prepare the medium containing released Cu ions, the medium containing CuO-NPs was incubated in a rotary shaker 37 °C for 24 h. The CuO-NP suspension was then centrifuged at 150 000g for 1 h to eliminate the NPs. The upper portion of supernatant was collected and used as medium containing Cu ions released from CuO-NPs.

To measure the concentration of Cu in the supernatant, the supernatant was ashed using nitric acid and perchloric acid and then diluted with water. The concentration was then measured using coupled plasma optical emission spectrometry (ICP-OES; SPS1700HVR, Seiko Instruments Inc., Chiba, Japan).

To study CuO-NPs in the cell culture medium, a grid for transmission electron microscopy (TEM) was immersed in the CuO-NP suspension (25 μg/mL) for 24 h and then dried in air. To confirm the removal of NPs by centrifugation, a TEM grid was immersed in the supernatant for 24 h and dried in air. The dark-field TEM images, elemental mapping, and energy-dispersive spectroscopy (EDS) spectrum were obtained by JEM-2100F (JEOL, Tokyo, Japan). The size of Cu-NPs after incubation for 24 h was examined scanning electron microscope (SEM) (S-4800, Hitachi High-Technology, Tokyo Japan).

Cell Culture. Carcinoma-derived human lung epithelial A549 cells were seeded in culture dishes and plates with DMEM at a concentration of 5000 cells/cm^2. Normal human small airway epithelial cells (SAEC, TaKaRa Bio, Tokyo, Japan) were seeded in basal medium (SAGM BulletKit, TaKaRa Bio) at a concentration of 2500 cells/cm^2. After culturing in medium at 37 °C in a 5% CO_2 humidified environment for 48 h, the cell concentration of this culture reached about 70% confluence. Next, the medium used to culture the cells was replaced with media containing CuO-NPs, released Cu ions, or $CuCl_2$. After culturing the cells for another 24 h, the cellular toxicity of the culture was evaluated. Six-well culture plates were used for the following: viable cell counts, calcein-AM staining, propidium iodide (PI) staining, TUNEL assay, DNA microarray, real-time quantitative PCR (qPCR), p38 and JNK inhibition, and siRNA-based gene knockdown. Ninety-six-well culture plates were used for the formazan formation assay. Furthermore, 35 mm glass bottom dishes were used for detecting mitochondrial damage.

Evaluation of Cytotoxicity. Cytotoxicity of the cells was evaluated by assessing viable cell counts and formazan formation. To count cells, cells were removed from cell plates by trypsin treatment after washing with PBS three times. These cells were centrifuged at 2000*g* for 2 min and then resuspended in DMEM. A hemocytometer was used to count viable cells not stained with trypan blue. To count the total number of cells, cells were visually counted in eight different areas for each of the four independently prepared rounds of cultures. To visualize whether a cell was dead or alive, cells on each plate were double-stained with calcein-AM and PI using the Cellstain Double Staining Kit (Dojindo, Kumamoto, Japan). Each stained cell was observed under a fluorescence microscope. To determine the ratio of apoptotic cells, harvested cells were fixed in ethanol and then stained with PI and FITC-labeled Annexin V. Fluorescent intensity was measured with flow cytometry (FACS Calibur, BD, NJ, USA). The level of formazan formed from the water-soluble tetrazolium salt (WST-8) was measured using Dojindo's Cell Counting Kit-8.

Observation of Internalized CuO-NPs. Cells exposed to CuO-NPs for 24 h were removed from culture plates by trypsin treatment and harvested by centrifugation at 2000*g* for 2 min. The cells were fixed with a mixture of 2% paraformaldehyde and 2.5% glutaraldehyde in 0.1 M cacodylate buffer (pH 7.4) for 2 h at room temperature. After a short rinse in the buffer, the samples were postfixed for 1 h in 1% OsO_4 in 0.1 M cacodylate buffer (pH 7.4). The samples were then rinsed in the buffer, dehydrated in a graded series of ethanol, and embedded in Spurr resin (Agar Scientific, England). Ultrathin sections were cut with an ultramicrotome (EM UC-6, Leica, Wetzlar, Germany) using a diamond knife. Sections were examined with a JEM-2100F (JEOL) for the dark-field TEM image and elemental mapping. Sections were stained with oolong tea extract (Oken Shoji, Tokyo, Japan), Ti blue (Oken Shoji), and lead citrate for observation with a field emission transmission electron microscope (JEM-3000F, JEOL).

Detection of Mitochondrial Damage. A549 cells were seeded at a concentration of 5000 cells/cm^2. After culturing for 48 h, CuO-NPs were added to the cells to obtain a concentration of 25 μg/mL, and the cells were cultured for an additional 4 h. This treatment was followed by the addition of $CuCl_2$ to obtain a concentration of 30 μg/mL, and the cells were further cultured. To detect mitochondrial damage, cells were stained with JC-1 (5,5′,6,6′-tetrachloro-1,1′,3,3′-tetrathylbenzinidazolylcarbocyanin iodide; Invitrogen, CA, USA), and mitochondria were detected using a confocal laser microscope. Damaged mitochondria accumulate less JC-1 and therefore exhibit less fluorescence.

DNA Microarray Analysis. Cells cultured previously in DMEM for 48 h were further cultured for 24 h in media containing CuO-NPs, released Cu ions, or in DMEM (control medium). Total RNA was then recovered from the cells in each culture using ISOGEN (Nippon Gene, Tokyo, Japan). These RNAs were amplified using Amino Allyl MessageAmp II aRNA Amplification Kit (Ambion, TX, USA) and then labeled with Cy3 and Cy5. Whole Human Genome Microarray Kit 4 × 44K (Agilent, CA, USA) was applied to the Cy3- and Cy5-labeled amplified RNAs, which were then competitively hybridized for 18 h at 65 °C. After washing this DNA microarray, the fluorescence intensity of Cy3 and Cy5 was scanned using GenePix 4000B (Molecular Devise, CA, USA) at 10 μm resolution at three levels, from a low PTM gain value to a high value. Spots in the scanned images were detected using GenePix Pro (Molecular Devise). The foreground and background median values of each spot were obtained from the median values of the pixels included in each spot area. The difference between the foreground and background values of each spot was established as the signal strength. The standard deviation of the background values was treated as the noise value. Only spots with signal values 3× the noise value or greater were considered valid spots. Data from scans, whose gains were separated into three levels, were globally normalized and merged. Finally, locally weighted scatterplot smoothing (LOWESS) adjustment was applied.

The DNA microarray experiment was carried out twice using RNA obtained from different cultures. For the first trial, RNA obtained from cells cultured in the control medium was labeled with Cy3. RNA obtained from cells cultured in media containing CuO-NPs and released Cu ions was labeled with Cy5. Genes whose Cy5 fluorescence intensity was 2× the fluorescence intensity of Cy3 or greater, or 0.5× the fluorescence intensity of Cy3 or lesser, were extracted as genes with altered expression levels. For the second trial, the roles of Cy3 and Cy5 were switched; that is, RNA obtained from the control cells was labeled with Cy5. Genes with altered expression level as indicated by the ratio of Cy3 to Cy5 fluorescence intensity were extracted. Of these extracted genes, only genes whose ratio of expression levels from the two trials was less than double the margin of error were identified as reproducible genes. The ratio of the expression levels of these genes was set as the average value of the two trials.

Next, these genes were placed into GO biological process categories using PANTHER gene expression analysis/compare gene lists (http://www.pantherdb.org/tools/genexAnalysis.jsp). Significant changes were indicated by categories with over(+) and p value <0.001.

Real-Time Quantitative PCR. Real-time quantitative PCR (qPCR) was performed to confirm the reproducibility of the ratio of RNA expression levels obtained from independent cultures for certain genes that revealed altered expression levels during the DNA microarray analysis. The primer sequence of each gene for qPCR is shown in Supporting Information (Table S10). The expression level of each gene was set as a value relative to the expression level of the GAPDH gene.

Western Blotting. The following primary antibodies were used for Western blotting: anti-GADD45B polyclonal antibody (ab105060, abcam, Cambridge, UK), anti-GADD45G polyclonal antibody (ab96578, abcam,), anti-NR4A1 monoclonal antibody (ab109180, abcam), anti-NR4A3 monoclonal antibody (WH0008013M6, Sigma-Aldrich), anti-CDC2 polyclonal antibody (9122, Cell Signaling Technology, MA, USA), anti-CCNB1 monoclonal antibody (ab72, abcam).

A549 cells were seeded at 5000 cells/cm^2 in 14.5 cm culture dishes containing DMEM. After 48 h, medium was replaced with media containing CuO-NPs, released Cu ions, or $CuCl_2$ and cultured for another 24 h. Total protein was extracted using RIPA buffer (Thermo Fisher Scientific, MA, USA) after cell washing with PBS buffer. Thirty micrograms of total protein was size fractionated on a precast SDS-polyacrylamide gel (15% acrylamide, Atto Corporation, Tokyo, Japan) and blotted onto an Immobilon-PSQ membrane (Millipore, MA, USA). After 1 h of blocking at room temperature with 3% immunoblot blocking reagent (Millipore), the membrane was incubated overnight at 4 °C with a primary antibody. The membrane was then washed three times with PBS buffer containing 0.05% Tween-20 and incubated for 1 h at room temperature or overnight at 4 °C with HRP-F(ab')2 goat anti-rabbit IgG(H+L) (Zymed Laboratories, CA, USA) or HRP goat anti-mouse IgG(H+L) (Zymed Laboratories). Proteins were detected using Immobilon Western chemiluminescent HRP substrate (Millipore).

Inhibition of JNK and p38. A549 cells were cultured in DMEM for 46 h. JIP-1 peptide (GIBCO) or SB239063 (Sigma-Aldrich), inhibitors of JNK and p38, respectively, was added so that the concentration of each reagent was 10 μM. After 2 h, these media were exchanged with media containing CuO-NPs, to which JIP-1 peptide or SB239063 was added to obtain the same concentration. The cells were cultured for another 24 h, and the number of live cells was counted.

Knock-Down of GADD45B and NR4A1 Using siRNA. The sequences of siRNAs used to knock down genes were the following: GADD45B sense (5′-GCACUUAUUCGAACCATT-3′) and antisense (5′-UGGUUCGAAUAACAAGUGCTT-3′); NR4A1 sense (5′-GCAUGGUGAAGGAAGUUGUTT-3′) and antisense (5′-ACAACUUCCUUCACCAUGCTT-3′). A549 cells were cultured in DMEM for 42 h, and each siRNA was added to the control medium to obtain a concentration of 25 μM. The siRNAs were introduced using Lipofectamine RNAiMAX (Invitrogen). After 6 h, the media were exchanged with medium containing CuO-NPs, and each siRNA was transfected. After culturing for 24 h, the number of viable cells was counted. Control cells were transfected with siRNA with the sequence of sense (5′-UCUUAAUCGCGUAUAAGGCTT-3′) and antisense (5′-GCCUUAUACGCGAUUAAGATT-3′).

***N*-Acetylcysteine (NAC) Treatment.** A549 cells were cultured in a 96-well plate or 35 mm^2 dish for 46 h, and NAC was added to the medium to obtain a concentration of 10 mM. After 2 h, the media were exchanged with medium containing CuO-NPs or released Cu ions. The cells were cultured another 24 h to examine recovery from toxicity.

Cell Cycle Analysis. Cells cultured previously in DMEM for 48 h were cultured for a further 24 h in media containing 25 μg/mL CuO-NPs, released Cu ions, or in DMEM (control medium). These cells were harvested, fixed in ethanol, and then stained with PI. Fluorescence intensity was measured with flow cytometry (FACS Calibur).

Statistics. Differences between samples and control were evaluated using two-tailed Student's t-test, and post hoc Bonferroni correction was performed for multiple comparisons. The results were considered significant if $p < 0.05$.

Acknowledgment. We thank Mr. S. Takenouchi, Ms. S. Kajiwara, Ms. H. Morita, Dr. X. Li, and Dr. E. Watanabe for technical assistance. We also thank Dr. H. Jiang, Institute of Chemistry, Chinese Academy of Sciences, for critical discussions. This work was supported by Grant-in-Aid from the Ministry of Health, Labour and Welfare of Japan.

Supporting Information Available: Tables S1–S9: Lists of genes. Table S10: Primer sequences. Figure S1: Particle size distribution of CuO-NPs (25 μg/mL) in culture medium. Figure S2: Preparation and characterization of medium containing Cu ions released from CuO-NPs. Figure S3: Cell viability as indicated by staining of cells that were exposed to CuO-NPs and the supernatant for 24 h with calcein acetoxymethyl ester (calcein-AM). Figure S4: Damage to mitochondria by CuO-NPs. Figure S5: Effect of nontoxic dummy Al_2O_3-NPs on supernatant toxicity. Figure S6: Internalized CuO-NPs observed by TEM. Figure S7: Western blotting analysis to confirm the change of gene expression. Figure S8: Cell cycle arrest due to CuO-NPs. Figure S9: Effects of SB239063 and JNK interacting protein 1 (JIP-1), which are inhibitors of p38 and JNK, respectively. Figure S10: siRNA knockdown efficiency of GADD45B and NR4A1. Figure S11: Effect of siRNA knockdown on the expression of GADD45B and NR4A1 on the cytotoxicity of CuO-NPs. Figure S12: CuO-NPs in dead cell observed by TEM. Figure S13: Cytotoxicity of CuO-NPs and Cu ions to primary human lung epithelial cells and change of gene expression. This material is available free of charge *via* the Internet at http://pubs.acs.org.

REFERENCES AND NOTES

1. Xu, M.; Fujita, D.; Kajiwara, S.; Minowa, T.; Li, X.; Takemura, T.; Iwai, H.; Hanagata, N. Contribution of Physicochemical Characteristics of Nano-oxides to Cytotoxicity. *Biomaterials* **2010**, *31*, 8022–8031.
2. Hanagata, N.; Xu, M.; Takemura, T.; Zhuang, F. Cellular Response to ZnO Nanoparticle Toxicity Inferred from Global Gene Expression Profiles. *Nano Biomed.* **2010**, *2*, 153–169.
3. Gabbay, J.; Borkow, G.; Mishal, J.; Magen, E.; Zatcoff, R.; Shemer-Avni, Y. Copper Oxide Impregnated Textiles with Potent Biocidal Activity. *J. Ind. Textiles* **2006**, *35*, 323–335.
4. Chang, H.; Jwo, C. S.; Lo, C. H.; Tsung, T. T.; Kao, M. J.; Lin, H. M. Rheology of CuO Nanoparticle Suspension Prepared by ASNSS. *Rev. Adv. Mater. Sci.* **2005**, *10*, 128–132.
5. Zhou, K.; Wang, R.; Xu, B.; Li, Y. Synthesis, Characterization and Catalytic Properties of CuO Nanoparticles with Various Shapes. *Nanotechnology* **2006**, *17*, 3939–3943.
6. Cioffi, N.; Ditaranto, N.; Torsi, L.; Picca, R. A.; Sabbatini, L.; Valentini, A.; Novell, L.; Tantillo, G.; Bleve-Zacheo, T.; Zambonin, P. G. Analytical Characterization of Bioactive Fluoropolymer Ultra-thin Coatings Modified by Copper Nanoparticles. *Anal. Bioanal. Chem.* **2005**, *381*, 607–616.
7. Xu, L.; Takemura, T.; Xu, M.; Hanagata, N. Toxicity of Silver Nanoparticles As Assessed by Global Gene Expression Analysis. *Mater. Exp.* **2011**, *1*, 74–79.
8. Ahamed, M.; Siddiqui, M. A.; Akhtar, M. J.; Ahmad, I.; Pant, A. B.; Alhadlaq, H. A. Genotoxic Potential of Copper Oxide Nanoparticles in Human Lung Epithelial Cells. *Biochem. Biophys. Res. Commun.* **2010**, *396*, 578–583.
9. Midander, K.; Cronholm, P.; Karlsson, H. L.; Elihn, K.; Moeller, L.; Leygraf, C.; Wallinder, I. O. Surface Characteristics, Copper Release, and Toxicity of Nano- and Micrometer-Sized Copper and Copper(II) Oxide Particles: A Cross-Disciplinary Study. *Small* **2009**, *5*, 389–399.
10. Karlsson, H. L; Cronholm, P; Gustafsson, J; Moeller, L. Copper Oxide Nanoparticles Are Highly Toxic: Comparison between Metal Oxide Nanoparticles and Carbon Nanotubes. *Chem. Res. Toxicol.* **2008**, *21*, 1726–1732.
11. Zhan, Q.; Lord, K. A.; Alamo, I., Jr.; Hollander, M. C.; Carrier, F.; Ron, D.; Kohn, K. W.; Hoffman, B.; Liebermann, D. A.; Fornace, A. J., Jr. The Gadd and MyD Genes Define a Novel Set of Mammalian Genes Encoding Acidic Proteins That Synergistically Suppress Cell Growth. *Mol. Cell. Biol.* **1994**, *14*, 2361–2371.
12. Fornace, A. J.; Jackman, J.; Hollander, M. C.; Hoffman-Liebermann, B.; Liebermann, D. A. Genotoxic-Stress-Response Genes and Growth Arrest Genes: Gadd, MyD, and Other Genes Induced by Treatments Eliciting Growth Arrest. *Ann. N.Y. Acad. Sci.* **1992**, *663*, 139–154.
13. Papathanasiou, M. A.; Kerr, N. C.; Robbins, J. H.; McBride, O. W.; Alamo, I., Jr.; Barrett, S. F.; Hickson, I. D.; Fornace, A. J., Jr. Mammalian Genes Coordinately Regulated by Growth Arrest Signals and DNA-Damaging Agents. *Mol. Cell. Biol.* **1989**, *10*, 4196–4203.
14. Zhang, W.; Bae, I.; Krishnaraju, K.; Azam, N.; Fan, W.; Smith, K.; Hoffman, B.; Liebermann, D. A. CR6: A Third Member in the MyD118 & Gadd 45 Gene Family Which Functions in Negative Growth Control. *Oncogene* **1999**, *18*, 4899–4907.
15. Beadling, C.; Johnson, K. W.; Smith, K. A. Isolation of Interleukin 2-Induced Immediate-Early Genes. *Proc. Natl. Acad. Sci. U.S.A.* **1993**, *90*, 2719–2723.
16. Liebermann, D. A.; Hoffman, B. MyD Genes in Negative Growth Control. *Oncogene Rev.* **1998**, *17*, 3319–3330.
17. Vairapandi, M.; Balliet, A. G.; Hoffman, B.; Liebermann, D. A. GADD45b and GADD45g Are cdc2/cyclinB1 Kinase Inhibitors with a Role in S and G2/M Cell Cycle Checkpoints Induced by Genotoxic Stress. *J. Cell Physiol.* **2002**, *192*, 327–338.
18. Wang, X. W.; Zhan, Q.; Coursen, J. D.; Khan, M. A.; Kontny, H. U.; Yu, L.; Hollander, M. C.; O'Connor, P. M.; Fornace, A. J., Jr.; Harris, C. C. GADD45 Induction of a G2/M Cell Cycle Checkpoint. *Proc. Natl. Acad. Sci. U.S.A.* **1999**, *96*, 3706–3711.

19. Jin, S.; Antinore, M. J.; Lung, F. D.; Dong, X.; Zhao, H.; Fan, F.; Colchagie, A. B.; Blanck, P. The GADD45 Inhibition of Cdc2 Kinase Correlates with GADD45-Mediated Growth Suppression. *J. Biol. Chem.* **2000**, *275*, 16602–16608.
20. Vairapandi, M.; Balliet, A. G.; Hoffman, B.; Liebermann, D. A. The Differentiation Primary Response Gene MyD118, Related to GADD45, Encodes for a Nuclear Protein Which Interacts with PCNA and *p21WAF1/CIP1*. *Oncogene* **1996**, *12*, 2579–2594.
21. Smith, M. L.; Chen, I. T.; Zhan, Q.; Bae, I.; Chen, C. Y.; Gilmer, T. M.; Kastan, M. B.; O'Connor, P. M.; Fornace, A. J., Jr. Protein Interaction of the p53-Regulated Protein Gadd45 with Proliferating Cell Nuclear Antigen. *Science* **1994**, *266*, 1376–1380.
22. Smith, M. L.; Ford, J. M.; Hollander, M. C.; Bortnick, R. A.; Amundson, S. A.; Seo, Y. R.; Deng, C.-X.; Hanawalt, P. C.; Fornace, A. J., Jr. p53-Mediated DNA Repair Responses to UV Radiation: Studies of Mouse Cells Lacking p53, p21, and/or Gadd45 Genes. *Mol. Cell. Biol.* **2000**, *20*, 3705–3714.
23. Smith, M. L.; Kontny, H. U.; Zhan, Q.; Sreenath, A.; O'Connor, P. M.; Fornace, A. J., Jr. Antisense GADD45 Expression Results in Decreased DNA Repair and Sensitizes Cells to U. V.-Irradiation or Cisplatin. *Oncogene* **1996**, *13*, 2255–2263.
24. Gupta, M.; Gupta, S. K.; Balliet, A. G.; Hollander, M. C.; Albert, J.; Fornace, A. J., Jr.; Hoffman, B.; Liebermann, D. A. Hematopoietic Cells from Gadd45a and Gadd45b Deficient Mice Are Sensitized to Genotoxic-Stress Induced Apoptosis. *Oncogene* **2005**, *24*, 7170–7179.
25. Gupta, M.; Gupta, S. K.; Hoffman, B.; Liebermann, D. A. Gadd45a gadd45b Protect Hematopoietic Cells from UV Induced Apoptosis *via* Distinct Signaling Pathways Including p38 Activation and JNK Inhibition. *J. Biol. Chem.* **2006**, *281*, 17552–17558.
26. De Smaele, E.; Zazzeroni, F.; Papa, S.; Nguyen, D. U.; Jin, R.; Jones, J.; Cong, R.; Franzoso, G. Induction of Gadd45β by NF-κB Downregulates Pro-apoptotic JNK Signalling. *Nature* **2001**, *414*, 308–313.
27. Amanullah, A.; Azam, N.; Balliet, A.; Hollander, C.; Hoffman, B.; Fornace, A.; Liebermann, D. Cell Signalling: Cell Survival and a Gadd45-Factor Deficiency. *Nature* **2003**, *424*, 741–742.
28. Takekawa, M.; Saito, H. A Family of Stress-Inducible GADD45-like Proteins Mediate Activation of the Stress-Responsive MTK1/MEKK4/MAPKKK. *Cell* **1998**, *95*, 521–530.
29. Selvakumaran, M.; Lin, H. K.; Miyashita, T.; Wang, H. G.; Krajewski, S.; Reed, J. C.; Hoffman, B.; Liebermann, D. Immediate Early Up-Regulation of Bax Expression by p53 But Not TGF beta 1: A Paradigm for Distinct Apoptotic Pathways. *Oncogene* **1994**, *9*, 1791–1798.
30. Selvakumaran, M.; Lin, H. K.; Tjin Tham Sjin, R.; Reed, J.; Liebermann, D.; Hoffman, B. The Novel Primary Response Gene MyD118 and the Proto-Oncogenes Myb, Myc and Bcl-2 Modulate Transforming Growth Factor b1-Induced Apoptosis of Myeloid Leukemia Cells. *Mol. Cell. Biol.* **1994**, *14*, 2352–2360.
31. Zhang, W.; Hoffman, B.; Liebermann, D. A. Ectopic Expression of MyD118/Gadd45/CR6 (Gadd45beta/alpha/gamma) Sensitizes Neoplastic Cells to Genotoxic Stress-Induced Apoptosis. *Int. J. Oncol.* **2001**, *18*, 749–757.
32. Yoo, J.; Ghiassi, M.; Jirmanova, L.; Balliet, A. G.; Hoffman, B.; Fornace, A. J., Jr.; Liebermann, D. A.; Bottinger, E. P.; Roberts, A. B. TGF-beta-Induced Apoptosis Is Mediated by Smad-Dependent Expression of GADD45B through p38 Activation. *J. Biol. Chem.* **2003**, *278*, 43001–43007.
33. Vairapandi, M.; Azam, N.; Balliet, A. G.; Hoffmann, D. A. Characterization of MyD118, Gadd45, and PCNA Impedes MyD/Gadd45 Mediated Negative Growth Control. *J. Biol. Chem.* **2000**, *275*, 16810–16819.
34. Azam, N.; Vairapandi, M.; Zhang, W.; Hoffman, B.; Liebermann, D. A. Interaction of CR6 (GADD45 gamma) with Proliferating Cell Nuclear Antigen Impedes Negative Growth Control. *J. Biol. Chem.* **2001**, *276*, 2766–2774.
35. Harkin, D. P.; Bean, J. M.; Miklos, D.; Song, Y. H.; Truong, V. B.; Englert, C.; Christians, F. C. Induction of GADD45 and JNK/SAPK-Dependent Apoptosis Following Inducible Expression of BRCA1. *Cell* **1999**, *97*, 575–586.
36. Kojima, S.; Mayumi-Matsuda, K.; Suzuki, H.; Sakata, T. Molecular Cloning of Rat GADD45gamma, Gene Induction and Its Role during Neuronal Cell Death. *FEBS Lett.* **1999**, *446*, 313–317.
37. Hildesheim, J.; Bulavin, D. V.; Anver, M. R.; Alvord, W. G.; Hollander, M. C.; Vardanian, L.; Fornace, A. J., Jr. Gadd45a Protects Against UV Irradiation-Induced Skin Tumors, and Promotes Apoptosis and Stress Signaling *via* MAPK and p53. *Cancer Res.* **2002**, *62*, 7305–7315.
38. Cazzalini, O.; Perucca, P.; Riva, F.; Stivala, L. A.; Bianchi, L.; Vannini, V.; Ducommun, B.; Prosperi, E. $p21^{CDKN1A}$ Does Not Interfere with Loading of PCNA at DNA Replication Sites, but Inhibits Subsequent Binding of DNA Polymerase δ at the G1/S Phase Transition. *Cell Cycle* **2003**, *2*, 596–603.
39. O'Connor, P. M. Mammalian G1 and G2 Phase Checkpoints. *Cancer Surv.* **1997**, *29*, 151–182.
40. Elledge, S. J. Cell Cycle Checkpoints: Preventing an Identity Crisis. *Science* **1996**, *274*, 1664–1672.
41. Kufer, T. A.; Sillje, H. H. W.; Koerner, R.; Gruss, O.; Meraldi, P.; Nigg, E. Human TPX2 Is Required for Targeting Aurora-A Kinase to the Spindle. *J. Cell Biol.* **2002**, *158*, 617–623.
42. Lu, B.; Yu, H.; Chow, C.; Li, B.; Zheng, W.; Davis, R. J.; Flavell, R. A. GADD45gamma Mediates the Activation of the p38 and JNK MAP Kinase Pathways and Cytokine Production in Effector TH1 Cells. *Immunity* **2001**, *14*, 583–590.
43. Yang, J.; Zhu, H.; Murphy, T. L.; Ouyang, W.; Murphy, K. M. IL-18-Stimulated GADD45 beta Required in Cytokine-Induced, but Not TCR-Induced, IFN-gamma Production. *Nat. Immunol.* **2001**, *2*, 157–164.
44. Angel, P.; Karin, M. The Role of Jun, Fos and the AP-1 Complex in Cell-Proliferation and Transformation. *Biochim. Biophys. Acta* **1991**, *1072*, 129–157.
45. Karin, M.; Liu, Z.-G.; Zandi, E. AP-1 Function and Regulation. *Curr. Opin. Cell Biol.* **1997**, *9*, 240–246.
46. Shaulian, E.; Karin, M. AP-1 in Cell Proliferation and Survival. *Oncogene* **2001**, *20*, 2390–2400.
47. Shaulian, E.; Karin, M. AP-1 As a Regulator of Cell Life and Death. *Nat. Cell Biol.* **2002**, *4*, E131–E136.
48. Li, Q. X.; Ke, N.; Sundaram, R.; Wong-Staal, F. NR4A1, 2, 3—An Orphan Nuclear Hormone Receptor Family Involved in Cell Apoptosis and Carcinogenesis. *Histol. Histopathol.* **2006**, *21*, 533–540.
49. Moll, U. M.; Marchenko, N.; Zhang, X.-K. p53 and Nur77/TR3-Transcription Factors That Directly Target Mitochondria for Cell Death Induction. *Oncogene* **2006**, *25*, 4725–4743.
50. Giono, L. E.; Manfreid, J. J. The p53 Tumor Suppressor Participates in Multiple Cell Cycle Checkpoints. *J. Cell. Physiol.* **2006**, *209*, 13–20.
51. Kastan, M. B.; Zhan, Q.; El-Deiry, W. S.; Carrier, F.; Jacks, T.; Walsh, W. V.; Plunkett, B. S.; Vogelstein, B.; Fornace, A. J., Jr. A Mammalian Cell Cycle Checkpoint Pathway Utilizing p53 and GADD45 is Defective in Ataxia-Telangiectasia. *Cell* **1992**, *71*, 587–597.
52. Guillouf, C.; Grana, X.; Selvakumaran, M.; Hoffman, B.; Giordano, A.; Liebermann, D. A. Dissection of the Genetic Programs of p53-Mediated G1 Growth Arrest and Apoptosis: Blocking p53-Induced Apoptosis Unmasks G1 Arrest. *Blood* **1995**, *85*, 2691–269.
53. Vogelstein, B.; Lane, D.; Levine, A. J. Surfing the p53 Network. *Nature* **2000**, *408*, 307–310.
54. Vousden, K. H. p53: Death Star. *Cell* **2000**, *103*, 691–694.
55. Andrews, G. K. Regulation of Metallothionein Gene Expression by Oxidative Stress and Metal Ions. *Biochem. Pharmacol.* **2000**, *59*, 95–104.
56. Huang, Y.-C. T.; Li, Z.; Carter, J. D.; Soukup, J. M.; Schwartz, D. A.; Yang, I. V. Fine Ambient Particles Induce Oxidative Stress and Metal Binding Genes in Human Alveolar Macrophages. *Am. J. Respir. Cell Mol. Biol.* **2009**, *41*, 544–552.
57. Min, K.-S.; Morishita, F.; Tetsuchikawahara, N.; Onosaka, S. Induction of Hepatic and Renal Metallothionein Synthesis by Ferric Nitrilotriacetate in Mice: The Role of MT as an Antioxidant. *Toxicol. Appl. Pharmacol.* **2005**, *204*, 9–17.
58. Kumari, M. V. R.; Hiramatsu, M.; Ebadi, M. Free Radical Scavenging Actions of Metallothionein Isoforms I and II. *Free Radical Res.* **1998**, *29*, 93–101.

Supporting Information

Molecular Responses of Human Lung Epithelial Cells to the Toxicity of Copper Oxide Nanoparticles Inferred from Whole Genome Expression Analysis

Nobutaka Hanagata[1,2,*], Fei Zhuang[2,3], Sarah Connolly[1,], Jie Li[1], Nobuhiro Ogawa[3] and Mingsheng Xu[4]**

[1]Nanotechnology Innovation Station, National Institute for Materials Science, 1-2-1 Sengen, Tsukuba, Ibaraki 305-0047, Japan
[2]Graduate School of Life Science, Hokkaido University, N10W8, Kita-ku, Sapporo 060-0812, Japan
[3]Biomaterials Unit, National Institute for Materials Science, 1-2-1 Sengen, Tsukuba, Ibaraki 305-0047, Japan
[4]State Key Laboratory of Silicon Materials, MOE Key Laboratory of Macromolecule Synthesis and Functionalization, and Department of Polymer Science and Engineering, Zhejiang University, Hangzhou 310027, P.R. China

* Corresponding author: Nobutaka Hanagata E-mail: HANAGATA.Nobutaka@nims.go.jp

Table of Contents